



# High-resolution mapping of time since disturbance and forest carbon flux from remote sensing and inventory data to assess harvest, fire, and beetle disturbance legacies in the Pacific Northwest

Huan Gu<sup>1</sup>, Christopher A. Williams<sup>1</sup>, Bardan Ghimire<sup>1</sup>, Feng Zhao<sup>2</sup>, and Chengquan Huang<sup>2</sup>

<sup>1</sup>Graduate School of Geography, Clark University, Worcester, MA 01610, USA

<sup>2</sup>Department of Geographical Sciences, University of Maryland, College Park, MD 20742, USA

Correspondence to: Huan Gu (hugu@clarku.edu, guhuan114031@gmail.com)

Received: 26 April 2016 – Published in Biogeosciences Discuss.: 17 May 2016

Revised: 20 October 2016 – Accepted: 9 November 2016 – Published: 25 November 2016

**Abstract.** Accurate assessment of forest carbon storage and uptake is central to policymaking aimed at mitigating climate change and understanding the role forests play in the global carbon cycle. Disturbances have highly diverse impacts on forest carbon dynamics, making them a challenge to quantify and report. Time since disturbance is a key intermediate determinant that aids the assessment of disturbance-driven carbon emissions and removals legacies. We propose a new methodology of quantifying time since disturbance and carbon flux across forested landscapes in the Pacific Northwest (PNW) at a fine scale (30 m) by combining remote sensing (RS)-based disturbance year, disturbance type, and above-ground biomass with forest inventory data. When a recent disturbance is detected, time since disturbance can be directly determined by combining three RS-derived disturbance products, or time since the last stand clearing can be inferred from a RS-derived 30 m biomass map and field inventory-derived species-specific biomass accumulation curves. Net ecosystem productivity (NEP) is further mapped based on carbon stock and flux trajectories derived from the Carnegie-Ames-Stanford Approach (CASA) model in our prior work that described how NEP changes with time following harvest, fire, or bark beetle disturbances of varying severity. Uncertainties from biomass map and forest inventory data were propagated by probabilistic sampling to provide a statistical distribution of stand age and NEP for each forest pixel. We mapped mean, standard deviation, and statistical distribution of stand age and NEP at 30 m in the PNW region. Our map indicated a net ecosystem productivity of  $5.9 \text{ Tg C yr}^{-1}$  for forestlands circa

2010 in the study area, with net uptake in relatively mature ( $>24$  years old) forests ( $13.6 \text{ Tg C yr}^{-1}$ ) overwhelming net negative NEP from tracts that had recent harvests ( $-6.4 \text{ Tg C yr}^{-1}$ ), fires ( $-0.5 \text{ Tg C yr}^{-1}$ ), and bark beetle outbreaks ( $-0.8 \text{ Tg C yr}^{-1}$ ). The approach will be applied to forestlands in other regions of the conterminous US to advance a more comprehensive monitoring, mapping, and reporting of the carbon consequences of forest change across the US.

## 1 Introduction

Disturbances profoundly alter ecosystems, often with legacies that persist for decades or centuries (Turner, 2010). Correspondingly, time since disturbance is a key determinant of ecosystem structure, composition, and function (Jenny, 1980; Chapin et al., 2012). It is also a primary control in many components of the forest carbon cycle, such as live biomass, coarse woody debris biomass, forest floor biomass, biomass accumulation, and so forth (Bradford et al., 2008). Considering time since disturbance is therefore essential for quantifying and predicting a wide range of ecological functions, including carbon stocks and fluxes, which are highly dynamic following disturbances, presenting a significant challenge for carbon budget assessment (Williams et al., 2014).

A number of prior studies have sought to incorporate the time since the last stand-clearing disturbance, analogous to forest stand age, as a determinant or predictor of carbon fluxes and stocks (Cohen et al., 1996; Chen et al., 2002,

2003; Law et al., 2004; Turner et al., 2004; Liu et al., 2011; Pan et al., 2011; Williams et al., 2012, 2014; Zhang et al., 2012). Data from the Forest Inventory and Analysis (FIA) offer one source for characterizing time since stand-replacing disturbances at broad scales (Williams et al., 2012, 2014). Stand ages were recorded by coring and dating of large trees in forest plots (FIA, 2015) because high-severity stand-replacement events that level all canopy dominants and even understory individuals leave a clearer mark of disturbance timing (Schoennagel et al., 2004). Above-ground live biomass also reflects the time since disturbance in so far as biomass exhibits a predictable rate of accumulation following stand replacement. The rate of biomass accumulation is influenced by a wide range of factors, such as climate, soil and site fertility, species composition, successional dynamics, the type of stand-replacement disturbance, and impacts from varying severity disturbance events (Johnson et al., 2000). The complex combination of how these factors are distributed across landscapes challenges generic characterization of time since disturbance and, most importantly, post-disturbance forest carbon dynamics. Though forest inventory remains one of the only ways of quantifying time since disturbance, it is an imperfect surrogate for time since disturbance at broad scales. However, because of low-severity, partial-disturbance events, time since disturbance can be difficult to quantify in field surveys.

Large-area fine-scale assessments of forest carbon stocks and fluxes require spatially extensive and continuous characterization of time since disturbance across landscapes at a scale that is able to detect small-scale disturbance events, typically around 100 m or less. FIA stand-age plot data can be used to create a continuous forest stand-age map at resolutions of 250 m in the conterminous US (Pan et al., 2011). However, such efforts are significantly limited by sparse plot coverage, poor representation of partial disturbances, and the fact that stand age, disturbance legacies, and carbon stocks and fluxes all vary widely at 250 m and coarser scales. Quantification of carbon stocks and fluxes based on coarse-scale stand-age information could be biased (Zhang et al., 2012). Thus, field inventory imputed carbon stocks and fluxes can only provide rough guidance for forest carbon management, monitoring, and verification at small scales (Wilson et al., 2013).

A number of remote sensing (RS) data and methods are available to quantify disturbance timing or disturbance timing-related attributes. Time series Landsat data and disturbance detection methods generate spatially extensive characterization of contemporary disturbance events and magnitude, providing a direct estimate of time since disturbance (Cohen et al., 2002; Goward et al., 2008; Huang et al., 2009, 2010; Zhu et al., 2012). However, such disturbance products only record events that occurred within the last several decades, thus missing the long-lasting legacies from disturbances that occurred before the beginning of the relevant remote sensing observations. Fortunately, such long-lasting

legacy effects are partially captured from RS-derived stand ages or above-ground biomass (Cohen et al., 1995; Saatchi et al., 2011; Kellndorfer et al., 2013). Stand-age maps directly determined from RS only offer rough age estimates binned into several classes over a large area, while above-ground biomass products estimated from optical, radar, and lidar data can provide pixel-level biomass (Cohen et al., 1995; Saatchi et al., 2011; Kellndorfer et al., 2013). Such above-ground biomass products have the potential to support inferences about additional properties of a given forest stand, such as stand age and disturbance legacy, particularly when considered within a well-defined regional context of typical biomass accumulation rates for a local set of edaphic, climatic, and forest-type settings (Zhang et al., 2014). There may be considerable ambiguity and confusion arising from incomplete information, as well as the potential for a range of field conditions that yield similar above-ground biomass or forest structure. Nonetheless, RS-derived forest biomass still provides a valuable way of characterizing the pixel-scale (e.g., 30 or 250 m) legacy effects of disturbance that occurred prior to RS observations, which is required for quantifying carbon stock recovery and carbon uptake and release rates over large areas. Combining disturbance products with other available disturbance layers is needed to distinguish among different disturbance types and severities to help assess carbon balance as a consequence of varying disturbance type and severity (Cohen et al., 2002).

Disturbance events are highly heterogeneous in space, with both occurrence and severity varying interactively with a wide range of site factors, resulting in highly diverse impacts on forest carbon dynamics (Turner, 2010). The effects of disturbances on forest carbon in US forests were assessed and simulated with time since disturbance from FIA data by a number of growth-based or process-based modeling approaches (e.g., Williams et al., 2016). This generates regional carbon stock and flux trajectories with time since disturbance following fire, bark beetle, and harvest with varying severity (Turner et al., 2004, 2007; Williams et al., 2012, 2014; Ghimire et al., 2012, 2015; Raymond et al., 2015). Previous studies that used model-derived trajectory curves to map carbon fluxes as a consequence of disturbances mainly focused on only one of the disturbance types, but accounting for multiple disturbance types is necessary for more accurately mapping and reporting carbon dynamics (Williams et al., 2016).

This study estimates and maps time since disturbance at a fine scale of 30 m from RS-derived products and FIA-derived biomass growth curves, and then maps net ecosystem productivity (NEP) based on disturbance history, time since disturbance, and carbon flux legacy. The specific objectives in this study are to (1) introduce a method for inferring a pixel's representative time since disturbance from RS-derived biomass and disturbance products at a 30 m resolution; (2) map NEP based on pre-existing, model-derived carbon stock and flux trajectories that describe how NEP changes with time following harvest, fire, or bark beetle dis-

turbances of varying severity; and (3) propagate uncertainties from RS-derived biomass products and FIA into uncertainty quantification of stand age and NEP. Our research represents an approach to map carbon stocks and fluxes at a high resolution across the conterminous US in support of national carbon monitoring, reporting, and management.

## 2 Materials and methods

### 2.1 Overview

Time since disturbance for each forest pixel was identified with one of the following two approaches depending on whether a recent disturbance was detected. The indicators of forest disturbances, including disturbance type and year, were determined from a combination of three RS-derived disturbance products based on assumed rules. For those pixels that have been mapped as having a recent disturbance since the beginning of the relevant RS observations, time since disturbance was directly estimated by the difference between the target mapping year (year 2010 in this study) and the year of the last observed disturbance. For forest pixels that were not disturbed during the time span of the disturbance product, we inferred time since last stand-clearing disturbance, which is also called “stand age” (Masek and Collatz, 2006); the terms “time since disturbance” and “stand age” are used interchangeably for recently undisturbed forest pixels thereafter. Stand age was inferred from RS-derived biomass data by finding the typical stand age that corresponds to each pixel’s biomass according to field-inventory-derived biomass-age curves, known as yield tables in forestry. The curves were sampled from FIA data and are specific to forest-type group and site-productivity class. Consequently, maps of forest-type group and site productivity aid pixel-level determination of which biomass-age curve is to be used for each pixel.

NEP in 2010 across the Pacific Northwest (PNW) region was mapped based on carbon stock and flux trajectories derived from the Carnegie-Ames-Stanford Approach (CASA) model in our prior work, describing how NEP changes with time following harvest, fire, or bark beetle disturbances of varying severity (Ghimire et al., 2012, 2015; Williams et al., 2014). NEP curves with time since disturbance vary by forest-type group and site-productivity class, and are unique to post-harvest (Williams et al., 2014), post-fire (Ghimire et al., 2012), and post-bark beetle (Ghimire et al., 2015) disturbance types. NEP trajectories were applied to pixels with attributes of time since disturbance, forest-type group, site-productivity class, disturbance type, and disturbance severity to estimate carbon fluxes in forests caused by post-disturbance growth and decomposition locally and regionally.

### 2.2 Inferring time since disturbance from remote sensing and inventory data

#### 2.2.1 Time since disturbance for disturbed forest pixels

North American Forest Dynamics (NAFD) disturbance products, Monitoring Trends in Burn Severity (MTBS), and aerial detection survey (ADS) polygons were used to determine whether and when forest pixels were disturbed from 1986 to 2010 (Table 1). NAFD products include 25 annual and 2 time-integrated forest disturbance maps with spatial resolution of 30 m for the conterminous United States (CONUS; Goward et al., 2015). These maps were derived from annual time series Landsat images from 1986 to 2010 using the vegetation change tracker (VCT) algorithm (Huang et al., 2009, 2010). In this paper, we used one of the time-integrated data layers, which maps the year of the most recent forest disturbance between 1986 and 2010. The MTBS project maps annual burned area and burn severity at 30 m resolution across all land of the United States from 1984 to 2014 (Eidenshink et al., 2007). Burned areas were determined by the differenced Normalized Burn Ratio (dNBR) index calculated across time series Landsat images. MTBS defines burn severity classes based on distribution of dNBR values and ecological settings. We integrated the annual MTBS data from 1986 to 2010 into two images: (1) year of the most recent fire event and (2) burn severity corresponding to the recent fire, and we applied a NAFD forest area mask to the integrated maps. The ADS program conducts annual surveys to investigate forest injury caused by insect outbreaks using aircraft observations since 1997, and it generates polygons recording a number of attributes, including disturbance year, and areas and number of trees killed by insects per area. We selected polygons attacked by bark beetles from 1997 to 2010, converted the number of trees killed by bark beetles per area to biomass killed per area by multiplying county-level FIA-derived average above-ground biomass per tree for corresponding forest types, and then binned biomass killed per area into different bark beetle severity levels (Ghimire et al., 2015). Those polygons were rasterized into two images with a cell size of 30 m: (1) year of bark beetle occurrence and (2) the severity of bark beetle outbreak represented by the amount of live biomass killed, with a NAFD forest mask applied to these two images.

Preprocessed layers of NAFD (Fig. 1a), MTBS (Fig. 1b), and ADS (Fig. 1c) data characterized the year of most recent disturbance events. These three layers were integrated to create a single 30 m resolution image of disturbance type associated with the last disturbance between 1986 and 2010. Since the NAFD disturbances have not yet been fully attributed to disturbance type, and because some pixels are recorded as having experienced more than one disturbance type, we made four simplistic rules to define a single disturbance type for each pixel. These assumptions are based on three rationales: (1) MTBS records most of the notable fire

**Table 1.** Data sources for inferring time since disturbance for recently disturbed and undisturbed forest pixels.

Data	Description	Source	Year	Input for recently disturbed and/or undisturbed forests
NAFD	Forest disturbance	Landsat	1986–2010	a, b
MTBS	Burned area and severity	Landsat	1986–2010	a
ADS	Area of insect outbreak and number of trees killed	Aerial survey	1997–2010	a
NBCD	Above-ground live biomass	Landsat, SRTM, FIA	2000	b
Forest-type group	Forest-type group	MODIS, NLCD, etc.	2001	b
Site productivity	Fraction of high productivity	FIA	1984–2014	b
Biomass-age curves	Biomass accumulation as a function of stand age	FIA	1984–2010	b

<sup>a</sup> Data are one of the inputs for inferring time since disturbance for recently disturbed forest pixels. <sup>b</sup> Data are one of the inputs for inferring time since disturbance for recently undisturbed forest pixels.

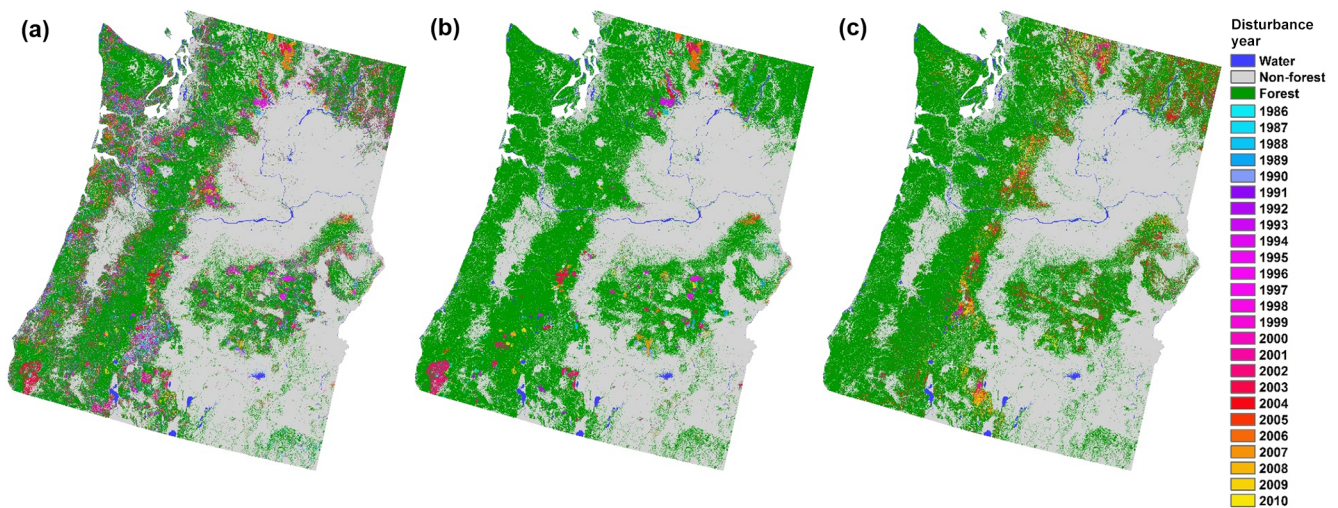


**Figure 1.** Year of last disturbance from (a) NAFD, (b) MTBS, and (c) ADS data of the PNW region. The time periods for NAFD, MTBS, and ADS datasets are 1986–2010, 1986–2010, and 1997–2010, respectively. NAFD: North American Forest Dynamics, MTBS: Monitoring Trends in Burn Severity, ADS: aerial detection surveys.

events in the region; (2) harvest events are one of the most ubiquitous stand-replacement disturbance types active in the region; (3) ADS-mapped polygons of bark beetle infestations often include unaffected stands, as has been reported in the literature (Meddens et al., 2012; Vanderhoof et al., 2014). Our four rules were (1) when NAFD and MTBS overlapped, if the two events were within 3 years of each other, we assigned fire to the pixel, and if the two were separated by more than 3 years, we assigned whichever event type was most recent with harvest for NAFD and fire for MTBS. (2) When NAFD and ADS overlapped, if the two events were separated by more than 3 years, harvest was assigned to the overlapping areas, but if they occurred within 3 years of each other, bark beetle outbreak was assigned. (3) When MTBS and ADS overlapped, the overlapping areas were assigned fire. (4) Harvest was assigned to all remaining disturbed pixels identified by NAFD. The year of last disturbance for each

disturbed pixel was then assigned based on the year of disturbance in each corresponding disturbance data product. Time since disturbance for disturbed pixels was then calculated as the difference between the target mapping year of 2010 and the year of last disturbance.

### 2.2.2 Time since disturbance for recently undisturbed forest pixels

For the remaining forest pixels that have no disturbance detected from 1986 to 2010, national biomass datasets were used to identify the corresponding stand age inferred from biomass-age curves that are specific to forest-type group and site-productivity classes (Table 1). Mapped strata of forest-type group and site productivity were used to determine the appropriate biomass-age curve to be used in referring stand age from biomass.

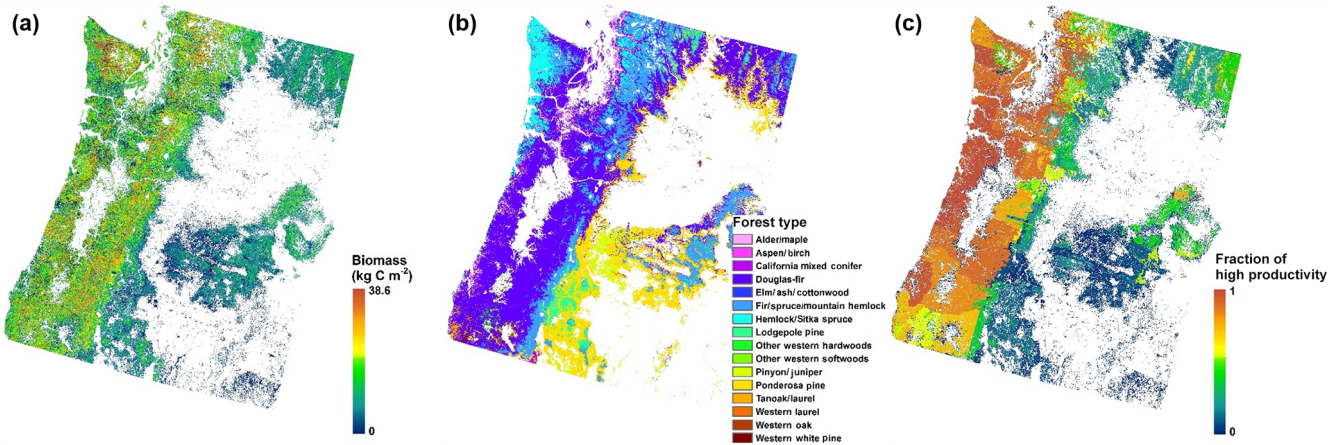


**Figure 2.** Maps of (a) NBCD 2000 (National Biomass and Carbon Dataset) above-ground biomass, (b) forest-type group and (c) site productivity in the PNW region.

Biomass-age curves were derived from the FIA database, sampled to provide means and sampling errors for two attributes: above-ground dry weight of live trees and area of forest land. The ratio of these two attributes provides above-ground live wood biomass per area. We obtained the ratios and associated errors for the PNW region through the USDA Forest Service FIA EVALIDator online tool (<http://apps.fs.fed.us/Evalidator/evalidator.jsp>). This yielded biomass per area within strata of forest-type group (28 classes), stand age (11 classes), and site productivity (7 classes); Table S1 in the Supplement. We combined the original seven site-productivity classes into high- and low-productivity classes, defined by the rate of forest volume growth as 8.4–15.7+ and 1.4–8.3 m<sup>3</sup> ha<sup>-1</sup> yr<sup>-1</sup>, respectively. Ratios and sampling errors were recalculated for each forest-type group, age class, and site productivity based on this grouping. Biomass-age curves were fitted following Williams et al. (2012) by parameterizing a wood production model that best matches the field inventory data. A Monte Carlo approach was used to incorporate uncertainty in the biomass per unit area with one hundred samples of the biomass at each age class drawn probabilistically. We then fitted corresponding one hundred curves for each forest type and productivity class, providing a distribution of biomass at each stand age from 1 to 200 years.

Pixel-level biomass was obtained from the National Biomass and Carbon Dataset for the year 2000 (NBCD 2000; Fig. 2a). The 30 m resolution biomass map was developed based on empirical modeling combining FIA data, InSAR data from 2000 SRTM, and Landsat ETM+ optical remote sensing (Kellndorfer et al., 2013). Only biomass estimates for undisturbed pixels were used for inferring stand age. Differences in forest masks between NAFD disturbance and NBCD biomass products led to a number of pixels having a biomass recorded as zero. These were replaced by the mean biomass of nearby undisturbed pixels with the same forest type and site productivity within this region. The

250 m forest-type group maps we used were created by the USDA Forest Service and were derived from MODIS composite images in combination with FIA data and nearly 100 other geospatial data layers, portraying 28 forest-type groups across the contiguous United States (Ruefenacht et al., 2008; Fig. 2b). Differences in map resolution between disturbance and forest-type maps led forest type to be undefined for some pixels along forest edges, so we assigned these the forest types of the nearest pixel. Site-productivity maps were also derived from FIA data (Fig. 2c) using the following procedure. The FIA dataset was sampled to obtain the area of each county across the region that is of each forest-type group and site-productivity class. We then created a continuous map of county numbers on a 0.01 degree grid, overlaid forest types, and integrated those with the data on each county's area of high- and low-productivity classes for the forest type that was most abundant in the pixel. This yielded a map of productivity class fractions, where each pixel has a fraction high productivity (summed over classes 1 to 3 spanning 8.4–15.7+ m<sup>3</sup> ha<sup>-1</sup> yr<sup>-1</sup>) and fraction low productivity (summed over classes 4 to 6 spanning 1.4–8.3 m<sup>3</sup> ha<sup>-1</sup> yr<sup>-1</sup>). In reality, site productivity is unlikely to vary across the 30 m pixel scale as much as it does at the county scale, whereas high- and low-site-productivity fractions are likely to vary across counties in some cases. However, an improved characterization is not available at this time.

For each recently undisturbed forest pixel, we extracted its biomass ( $B$ ), forest type ( $T$ ), and fraction of high productivity ( $f_{\text{high}}$ ), and then retrieved 100 biomass trajectories for forest type  $T$  and for high- and low-productivity classes, respectively. If the pixel was located at a high-productivity site ( $f_{\text{high}} = 1$ ), we treated 100 biomass curves for high productivity as 100 biomass realizations at stand ages from 0 to 200. All the biomass values among those realizations that lie within 20 % of the pixel's observed  $B$  were pooled and corresponding stand ages were derived (Fig. 3a). We then cal-

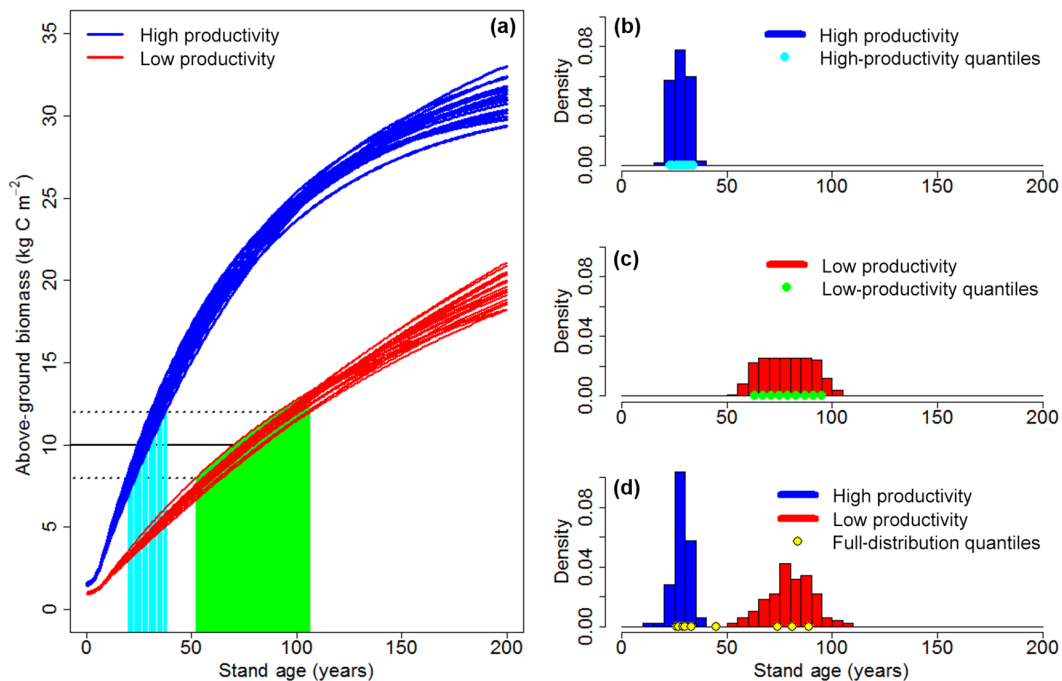


**Figure 3.** Stand age inferred based on field-inventory-derived species-specific biomass-age curves (a) for a forest pixel of the same forest-type group with above-ground biomass of  $10 \text{ kg C m}^{-2}$  and having no recent disturbance. Histogram and quantiles of stand ages are shown for three site-productivity classes: (b) high-productivity site ( $f_{\text{high}} = 1$ ), (c) low-productivity site ( $f_{\text{high}} = 0$ ), and (d) mixture of high- and low-productivity sites ( $f_{\text{high}} = 0.6$ ).

culated the mean, standard deviation, and each of the 10th quantiles from the pooled stand ages (10th, 20th, 30th, ..., 80th, 90th quantiles of stand age; Fig. 3b). The quantiles provided a frequency distribution of stand age for the individual pixel. Similarly, if the pixel was entirely of low site productivity ( $f_{\text{high}} = 0$ ), we followed the steps above but used trajectories for low-productivity classes to derive stand age distribution for low productivity (Fig. 3c). In reality,  $f_{\text{high}}$  is almost always between 0 and 1 (maximum  $f_{\text{high}} = 0.996$ , minimum  $f_{\text{high}} = 0.015$  in PNW). In order to reflect high–low productivity proportion of the total, we combined the two distributions above (one for high- and the other for low-productivity classes) by making copies of the two distributions with  $10 \times f_{\text{high}}$  copies for high productivity and  $10 \times (1 - f_{\text{high}})$  copies for low productivity. We calculated the mean, standard deviation, and quantiles from the combined distribution of stand age (Fig. 3d). Since 2010 was the target year for our mapping of stand age and carbon fluxes, while biomass maps were generated for the year 2000, we simply added 10 years to the inferred ages to get adjusted stand ages. Using the procedure above across all undisturbed forest pixels, we generated maps of the mean and standard deviation of stand age.

Finally, we merged the stand-age map for undisturbed forest pixels with the time since disturbance map for disturbed pixels to obtain a continuous map for all the forest pix-

els across the study area. To evaluate the derived map of time since disturbance, we made comparisons with two currently available products. First, density curves of stand age were plotted with maps derived from this study and Pan et al. (2011) for the study area. Another comparison was made between the distribution of forest area with age class from this study and that sampled from the FIA dataset.

### 2.3 Estimating NEP and uncertainties across the PNW region

#### 2.3.1 Carbon flux trajectories for harvest, fire and bark beetle

Carbon flux trajectories for post-harvest, -fire, and -bark beetle outbreaks were derived from our prior work (Ghimire et al., 2012, 2015; Williams et al., 2014) involving an inventory-constrained version of the CASA carbon cycle process model with inclusion of disturbance processes. The CASA model used here is based on Randerson et al. (1996) and operates on a monthly time step. It uses a light-use efficiency approach for simulating net primary productivity (NPP) based on RS-derived absorption of photosynthetically active radiation, biome parameters, and climate data. The model then allocates NPP to three live carbon pools (leaves, roots, and wood) and transfers carbon to dead pools (litter and soils) based on biome-specific rates of tissue turnover.

Carbon in dead organic matter pools is transferred between pools (surface structural C, surface metabolic C, soil structural C, soil metabolic C, above-ground coarse woody debris C, belowground coarse woody debris C, surface microbial C, soil microbial C, slow C, and passive C; Fig. S1 in the Supplement). Amounts of carbon transferred to microbial pools and carbon emitted to the atmosphere from microbial decomposition of soil and litter, i.e., heterotrophic respiration (Rh), depend on the rate and efficiency of heterotrophic consumption, which varies between pools in the model and also depends on biome- and pool-specific chemistry and site-specific climate setting, such as soil moisture and temperature. The difference between NPP and summed Rh of the 10 detrital pools is then calculated as NEP. Above-ground biomass-age curves sampled from the FIA database were used as a constraint to adjust wood turnover rate (mortality and shedding) and default output NPP by a scalar parameter, which therefore influences accumulation of live biomass and the amount of carbon allocated to live and dead pools. The adjustment of those CASA parameters was performed for each specific combination of forest-type group and site-productivity class. Implementation of the model involved a simulation sequence that began with spin-up to equilibrium carbon pools using FIA-adjusted NPP, which was followed by a pre-disturbance with ensuing regrowth to a set of pre-disturbance ages, and lastly, imposition of the disturbance of interest to generate flux and stock dynamics in response to harvest, fire, or beetle outbreak disturbance types at different severities. The fate of carbon influenced by disturbances varied by disturbance type as described below. Disturbance types considered in the model included stand-replacing harvest, fire, and bark beetle outbreaks, with full descriptions of the carbon dynamics in pools after a disturbance provided in Ghimire et al. (2012, 2015), Williams et al. (2014), and described further below.

Model treatments of disturbance impacts to the carbon cycle were as follows. For all disturbance type cases, a post-disturbance decline and ensuing recovery of NPP and fractional allocation to wood were modeled as a negative exponential function of time since disturbance, recovering to the pre-disturbance level within 8 years (Williams et al., 2012). The mortality and fate of disturbance-killed and/or -combusted carbon pools differed by disturbance type. For harvest (Williams et al., 2014), the post-disturbance biomass was set to 50 % of the above-ground live wood biomass reported in FIA data for the 0 to 20 year-old age class, regardless of the pre-disturbance biomass condition. Harvest-killed live wood, leaves, and roots were calculated from their corresponding fractions of pre-disturbance to post-disturbance conditions. Of the disturbance-killed above-ground live wood, 80 % was assumed to have been removed from the site, with the remainder being treated as slash subject to decomposition as coarse woody debris. All leaves of disturbance-killed trees are assumed to decompose on-site. All belowground wood that succumbs to mortality en-

ters a belowground coarse woody debris carbon pool. For fire (Ghimire et al., 2012), disturbance kill is portrayed as a partial-mortality event in which fires reduce pre-fire live biomass pools based on the fractional tree mortality, which varies by forest-type group and fire-severity class (high, medium, or low to match the MTBS dataset). The amount of live biomass remaining after a fire is calculated from the fraction of vegetation mortality emerging from an extensive literature survey. Fire-killed material is either directly combusted and released to the atmosphere or transferred to dead carbon pools. The same applies to foliage and root mortality, though roots are not directly combusted. Fire-killed trees enter a new standing dead pool in the model with a fast turnover fall rate of 10 years post fire with transfer to the coarse woody debris pool. Litter and soil organic carbon in the upper soil layers were also vulnerable to combustion. All of these rates were based on literature review (Ghimire et al., 2012). For bark beetle outbreaks (Ghimire et al., 2015), beetle-killed biomass was simulated for a wide range of intensities from near zero to 100 % mortality to generate a family of curves that could be applied in the mapping stage. Beetle attack caused leaf carbon to enter the surface litter pool, above-ground wood to enter a snag pool, and belowground wood and fine root to enter corresponding soil carbon pools. The portions killed for each were based on the percent mortality imposed for each severity level being simulated, which was derived from the ratio of the biomass at the midpoint of each severity class (of 1680 levels of intensity) to the pre-disturbed above-ground biomass values corresponding to the mean age of a given forest type under attack (Ghimire et al., 2015). Soil carbon pools respond to all of these dynamics according to the model's climate-mediated turnover times for each carbon pool, and the associated carbon flows (Fig. S1).

For a given forest type, site productivity, and prior disturbance, this forest disturbance version of the CASA model simulates NPP, Rh, and NEP as a function of time since disturbance. A family of curves describing carbon stocks in carbon pools (soil organic carbon, litter, slow turnover soil carbon, above-ground coarse woody debris, belowground coarse woody debris, and total live woody biomass), NPP, Rh, and NEP with time since disturbance for each combination were created to represent uncertainties in the amount of biomass killed and left on site after a disturbance, the amount of biomass left live on site post-disturbance, and the rate of biomass accumulation and mortality (Ghimire et al., 2012, 2015; Williams et al., 2014). This study emphasized the use of NEP curves from our prior works combined with time since disturbance derived from this study to map spatially explicit NEP in the PNW region. Fig. 4 provides examples of post-disturbance NEP trajectories from our prior work, showing the average of 20 simulations of post-harvest NEP (Fig. 4a, d), the average of 25 simulations of post-fire NEP for three different fire severities (Fig. 4b, e), and one simulation of post-bark beetle NEP for three examples of bark beetle disturbances that kill low, medium, and high amounts

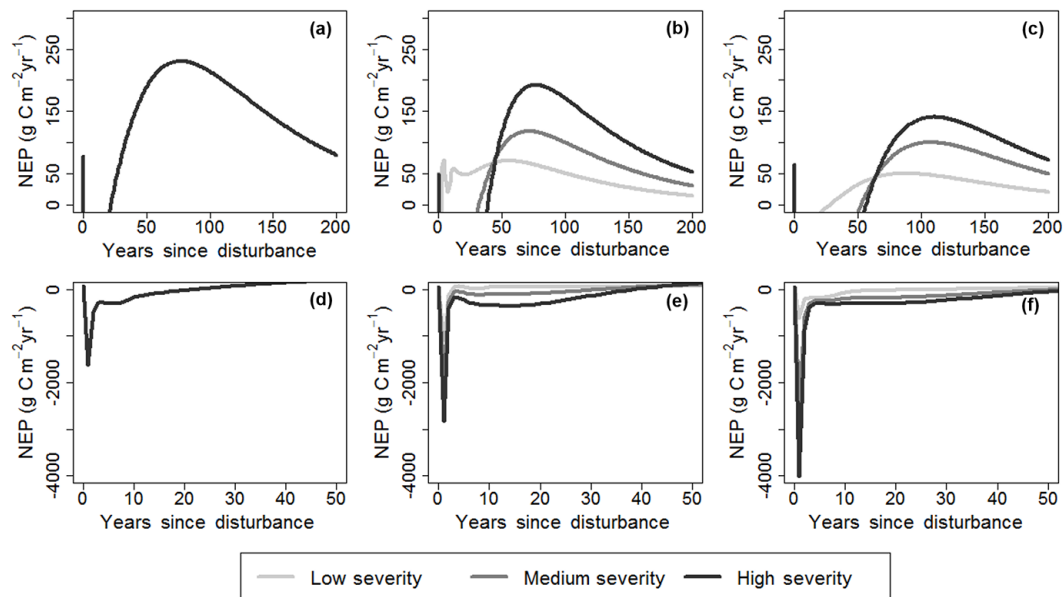


**Figure 4.** Carbon flux trajectories of (a, d) post-harvest (Williams et al., 2014), (b, e) post-fire (Ghimire et al., 2012), and (c, f) post-beetle (Ghimire et al., 2015) for a range of severities in high-site-productivity Douglas-fir stands of the PNW region. The typical pattern of NEP following a disturbance involves a large negative value immediately after disturbance, a rise for a number of years to reach a maximum rate of carbon uptake, and then a gradual decline to a steady state.

**Table 2.** Area (ha) of all forest lands, forests disturbed by harvest (1986–2010), fire (1986–2010), and bark beetle (1997–2010) by forest-type group, and for high- and low-site-productivity class in the PNW region.

Forest-type group*	All forests		Harvested		Burned		Bark beetle infested	
	High	Low	High	Low	High	Low	High	Low
Douglas-fir	6 909 151	3 097 083	2 039 661	752 902	161 221	181 147	301 234	41 6181
Ponderosa pine	565 633	2 953 701	188 300	888 668	39 135	213 925	53 982	26 1530
Fir/spruce/mountain hemlock	1 220 916	1 914 562	155 898	250 135	61 140	135 947	193 838	343 326
Hemlock/Sitka spruce	1 168 836	211 376	338 263	45 762	255	226	54 352	19 382
Pinyon/juniper	79 800	664 050	10 561	84 517	2988	27 601	250	1378
Alder/maple	633 369	43 005	278 797	18 128	325	24	3442	290
Lodgepole pine	135 874	441 717	38 737	167 320	13 064	42 235	22 692	78 753
Western oak	52 774	97 472	15 572	25 392	4371	7817	1036	2026
California mixed conifer	16 841	73 817	5017	18 369	550	1669	836	1376
Tanoak/laurel	50 897	26 536	11 291	5351	6431	3509	265	160
Other western hardwoods	39 696	33 718	10 542	7342	535	844	912	777
Elm/ash/cottonwood	34 093	17 945	14 779	7812	331	284	60	41
Western larch	20 464	28 342	3126	4611	744	1436	5078	6597
Other western softwood	9956	24 206	1441	2587	1711	6037	1726	5259
Western white pine	7877	4471	204	183	7360	3951	35	37
Aspen/birch	1908	2607	730	894	176	286	124	353

\* Forest-type groups are ordered by forest area from largest to smallest.

of biomass (Fig. 4c, f) in high-site-productivity Douglas-fir stands in the PNW region. The typical overall pattern of NEP following a disturbance involves a large negative value immediately after the disturbance, a rise for a number of years to reach a maximum rate of carbon uptake, and then a gradual decline to a steady state. The post-disturbance

NEP curves across all forest types, productivity classes, and disturbance types are presented in the Supplement figures (Figs. S2, S3, S4, S5, S6), Rh trajectories are shown in Figs. S7, S8, S9, S10, S11, and characteristic trajectories of post-disturbance carbon stocks in carbon pools are provided

as well (Figs. S12, S13, S14, S15, S16, S17 for harvest as an example).

### 2.3.2 Mapping NEP and uncertainties across the PNW region

The characteristic trajectories serve as look-up tables relating carbon fluxes and stocks (here just NEP) to years since disturbance within the strata of forest-type group, site-productivity fraction, disturbance type, and severity. For disturbed pixels, the distribution of NEP corresponding to the pixel's time since disturbance and forest type was sampled for both high- and low-productivity classes. It was then weighted according to the pixel's fraction of high site productivity ( $f_{\text{high}}$ ). Weighting involved a simple repetition of each data population based on the pixel's fraction of high productivity, with  $10 \times f_{\text{high}}$  copies for the high-productivity estimates and  $10 \times (1 - f_{\text{high}})$  copies for the low-productivity population. These two populations were then combined to create a single composite distribution representing the full probability distribution for the pixel's NEP. A similar procedure was performed for all remaining undisturbed forest pixels but including the additional uncertainty on the pixel's stand age. We propagated stand-age uncertainty by obtaining the NEP distribution for each of the 10th quantiles of the age distribution corresponding to the pixel's biomass and forest type for both high- and low-productivity classes and compositing these into a full probability distribution of the pixel's NEP based on the pixel's fraction of high probability ( $f_{\text{high}}$ ). Finally, we calculated the mean, standard deviation, and quantiles (10th, 20th, 30th, ..., 80th, 90th quantiles) of NEP distribution for each forest pixel across the PNW region.

## 3 Results

### 3.1 Disturbance maps derived from NAFD, MTBS, and ADS

Across the  $2.1 \times 10^7$  ha of forest in the PNW region, harvest was recorded as having affected the largest area ( $5.4 \times 10^6$  ha from 1986 to 2010), followed by bark beetles ( $1.8 \times 10^6$  ha from 1997 to 2010), and then fire ( $9.3 \times 10^5$  ha from 1986 to 2010). Their distributions are displayed in Fig. 5. Reported as percentages, harvest, bark beetles, and fire affected 26, 9, and 5 % of all forestland in the PNW during their respective time intervals. Table 2 provides an additional report of each area by forest-type group and for high- and low-productivity-class sites. Douglas-fir comprises nearly 50 % of all forest in the PNW, with about 70 % of it being in high-productivity-class lands. Ponderosa pine, fir-spruce-mountain hemlock, and hemlock-Sitka spruce are the next most abundant forest-type groups, comprising 17, 15, and 7 % of the PNW forest, with 16, 39, and 85 % in high-productivity sites, respectively.

About half (52 %) of all harvesting occurred in Douglas-fir forests, with 20 % in ponderosa pine stands and 8 and 7 % in fir-spruce-mountain hemlock, and hemlock-Sitka spruce stands. Of all forestland that burned, 37 % was in Douglas-fir stands, 27 % in ponderosa pine, and 21 % in fir-spruce-mountain hemlock. Hemlock-Sitka spruce was not vulnerable to fire. Though fire affected a larger area of low-productivity sites for ponderosa pine and fir-spruce-mountain hemlock forest types, fire occurrence was equally likely across low- and high-productivity classes. In contrast, Douglas-fir stands had similar burned areas for low- and high-productivity sites, but low-productivity sites were 3 times as likely to experience fire. Bark beetle outbreaks were most common in Douglas-fir stands, with 40 % of all of the outbreak area, while 30 and 18 % occurred in fir-spruce-mountain hemlock and ponderosa pine stands, respectively. As with fire, though a larger proportion of the total bark beetle outbreak area occurred in low-productivity ponderosa pine and fir-spruce-mountain hemlock stands, their occurrence was equally likely across low- and high-productivity sites. Again in contrast, bark beetle outbreak areas for low- and high-productivity classes are similar in Douglas-fir forests, but beetle outbreak occurrence was about 3 times more likely in low-productivity sites. Of all Douglas-fir stands, 28 % were disturbed by harvest, 3 % by fire, and 7 % by bark beetles. Percentages for ponderosa pine stands were 31, 7, and 9 % for harvest, fire, and bark beetles, respectively. For fir-spruce-mountain hemlock they were 13, 6, and 17 %, respectively, and hemlock-Sitka spruce was mainly disturbed by harvesting (28 %), with 0 % for fire and 5 % for bark beetles.

### 3.2 Biomass-age curves by forest-type group and site-productivity class

The fitted biomass regrowth curves exhibit considerable variations across forest type and site-productivity class (Fig. 6 for Douglas-fir, ponderosa pine and fir-spruce-mountain hemlock). Compared to Douglas-fir forests, ponderosa pine forests hold only about 28 to 33 % as much biomass, and fir-spruce-mountain hemlock forests hold about 59 to 64 % as much. Biomass accumulates more rapidly and to a higher maximum stock for high-productivity sites for all forest types according to FIA data and corresponding model fits, achieving about 1.4 to 1.8 times the biomass at low-productivity sites. However, the biomass-age curves share some common features among different forest types and site-productivity classes. Biomass accumulates rapidly at early ages ( $\sim 0$ –50 years), slowing down with age until it saturates, often around 150–200 years. Furthermore, variation in biomass increases as a function of stand age both in the FIA data and in the model fits. The fitted curves provided a range and distribution of biomass at each stand age from 0 to 200 years. Because of the simple stand-level growth equation that was assumed, these curves yielded a smoothed fit to the inventory

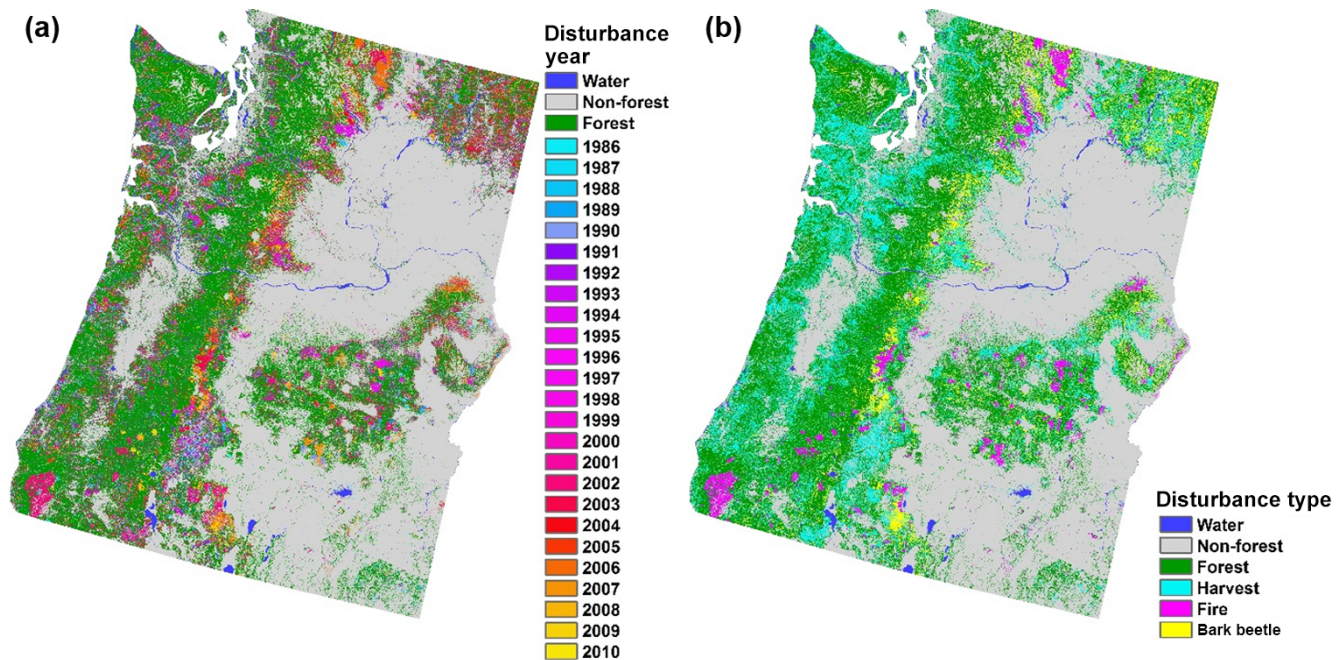


**Figure 5.** Maps of (a) disturbance year and (b) disturbance type integrated from NAFD (Fig. 1a), MTBS (Fig. 1b), and ADS (Fig. 1c) data in the PNW region. NAFD: North American Forest Dynamics, MTBS: Monitoring Trends in Burn Severity, ADS: aerial detection survey.

data rather than the erratic and fluctuating jumps imposed on the general increase of stand age seen in the field data.

### 3.3 Maps of time since disturbance and uncertainties across the PNW region

The forested landscape is a complicated mosaic of time since the last disturbance (Fig. 7a). Overall, a wide range of years are spanned, with abrupt discontinuities related to recent stand-replacement disturbances, transitions between forest types, and transitions between site-productivity classes. One feature that stands out prominently is the prevalence of recent disturbances along the eastern, drier side of the Cascade Range, resulting from both harvesting and bark beetle outbreaks (Fig. 5b). Large fires produced sizable patches with the same time since disturbance. The imprint of segments of relatively old, high-elevation forests is also evident. It should be noted that this map was not used directly in the computation of NEP for undisturbed forest pixels, which relied instead on stand-age distributions for high- and low-site-productivity classes, but it is presented here to provide a best estimate of disturbance timing at the pixel scale.

Uncertainty on the time since disturbance for disturbed forest pixels is not currently available from disturbance products and thus was not mapped. For undisturbed forest pixels, the uncertainty of stand age was represented by standard deviation of the full stand-age distribution combined from high and low site productivity and reflecting high–low productivity proportion. The uncertainty map identifies locations where stand age is more tightly constrained by the data and

method (Fig. 7b). Across all the stand ages inferred from the biomass data (undisturbed forest pixels), the spatially averaged mean standard deviation of stand age is around 25 years.

Density curves of stand age were compared between maps derived from this study and from Pan et al. (2011) for the study area. In undisturbed areas, spatial pattern and density distribution of stand age between the two studies are mostly consistent (Fig. 9a, b), but this study has a much higher density at the age class of 0–10 years and a bit lower density at 50–100 years (Fig. 9c). Furthermore, the distribution of forest area with age class from this study was compared with that sampled from the FIA dataset (Fig. 10 for Douglas-fir and fir–spruce–mountain hemlock). We provided two age distributions from this study, one sampled from only undisturbed pixels and another including all forested pixels. Overall, the pattern of FIA-derived age distribution matches well with that derived from our study, but with our study having consistently lower forest areas of age classes larger than 20 years. This is true except for in the youngest age classes when we include the pixels marked as disturbed in this study, finding a much larger frequency of young forests.

### 3.4 Maps of NEP and uncertainties across the PNW region in 2010

Spatial variations in mean annual NEP are determined by differences in strata of time since disturbance, forest-type group, and site productivity used in the mapping procedure (Fig. 8a). There is a general pattern of weaker carbon sinks in the eastern portion of the study area. Both sink strength and

**Table 3.** Mean net ecosystem productivity (NEP) and total net carbon uptake by forest-type group in all forests, recently undisturbed forests, forests disturbed by harvest, fire, and bark beetle, which occurred during the time span of remote sensing disturbance products.

Forest-type group*	All forests		Recently undisturbed		Harvested		Burned		Bark beetle infested	
	Mean NEP (g C m <sup>-2</sup> yr <sup>-1</sup> )	Total NEP (Gg C yr <sup>-1</sup> )	Mean NEP (g C m <sup>-2</sup> yr <sup>-1</sup> )	Total NEP (Gg C yr <sup>-1</sup> )	Mean NEP (g C m <sup>-2</sup> yr <sup>-1</sup> )	Total NEP (Gg C yr <sup>-1</sup> )	Mean NEP (g C m <sup>-2</sup> yr <sup>-1</sup> )	Total NEP (Gg C yr <sup>-1</sup> )	Mean NEP (g C m <sup>-2</sup> yr <sup>-1</sup> )	Total NEP (Gg C yr <sup>-1</sup> )
Douglas-fir	14.9	1489.2	128.6	7912.6	-205.7	-5745.7	-130.0	-445.0	-32.9	-235.0
Ponderosa pine	16.9	594.2	47.4	887.9	-14.8	-159.2	-3.0	-7.7	-40.4	-127.1
Fir/spruce/mountain hemlock	52.6	1649.7	108.3	2161.6	-22.0	-89.5	-35.0	-69.0	-66.2	-354.7
Hemlock/Sitka spruce	107.5	1483.5	197.0	1816.6	-76.7	-294.6	-106.3	-0.5	-52.1	-38.3
Pinyon/juniper	5.2	39.0	9.4	58.2	-18.7	-17.8	-1.9	-0.6	-48.7	-0.8
Alder/maple	58.4	395.3	118.0	442.8	-16.7	-49.7	97.6	0.3		
Lodgepole pine	9.6	55.7	36.6	78.6	4.2	8.6	28.2	15.6	-46.4	-47.0
Western oak	9.5	14.2	28.4	26.7	-33.9	-13.9	5.8	0.7		
California mixed conifer	14.4	13.1	27.0	17.0	-19.5	-4.6	70.3	1.6	-51.4	-1.0
Tanoak/laurel	79.0	61.2	161.8	81.6	-82.3	-13.7	-73.4	-7.3		
Other western hardwoods	43.7	32.1	62.0	32.5	-12.4	-2.2	59.5	0.8		
Elm/ash/cottonwood	29.9	15.6	119.4	34.3	-81.6	-18.4	-61.6	-0.4		
Western larch	35.9	17.5	97.2	26.5	-34.7	-2.7	-21.1	-0.5	-50.0	-5.8
Other western softwood	-12.9	-4.4	26.4	4.1	-21.8	-0.9	-39.9	-3.1	-64.5	-4.5
Western white pine	35.9	4.4	4.8	0.0	-14.6	-0.1	39.8	4.5	-53.3	0.0
Aspen/birch	20.3	0.9	51.6	1.0	-14.8	-0.2	-9.8	0.0		
Total	28.5	5861.2	108.8	13581.8	-118.8	-6404.5	-55.1	-510.5	-46.2	-814.2

\* Forest-type groups are ordered by the forest area from largest to smallest.

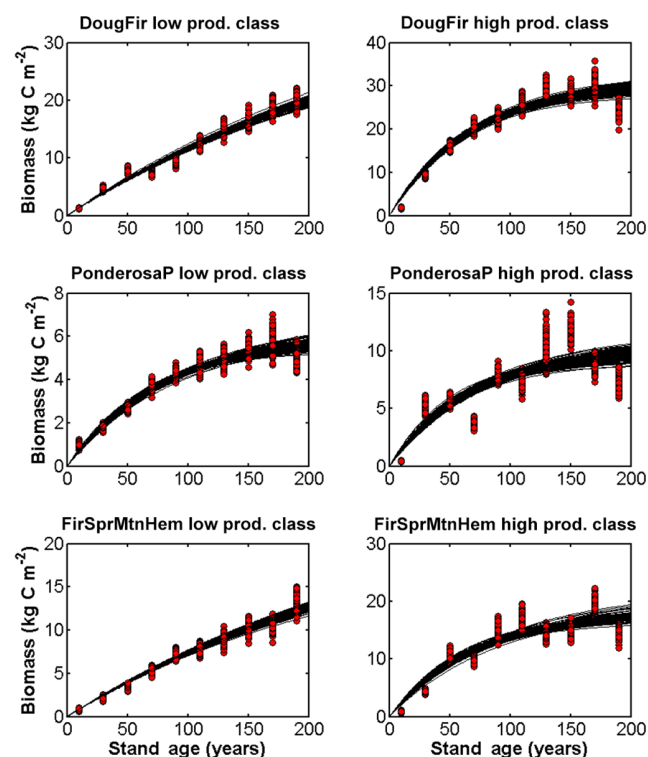


**Figure 6.** Biomass-age curves sampled from FIA data for each forest-type group and site-productivity class in the PNW region. Curves for the three most abundant forest-type groups are shown (DougFir is Douglas-fir, Ponderosa P is ponderosa pine, and FirSprMtnHem is fir/spruce/mountain hemlock). Red dots are independent samples drawn probabilistically from the FIA data.

carbon source strength tend to be largest in western areas of higher biomass. Recent (<20 years) fire and harvest disturbances tend to create focused carbon sources on the landscape, giving way to sinks as regrowth ensues. For example, one can see a clear imprint of the well-known 2002 Biscuit Fire in southwestern Oregon (bottom left of Fig. 8a, also refer to bottom left of Fig. 5a and b). Area with very recent but low-severity bark beetle outbreaks have only a muted reduction in NEP compared to nearby undisturbed forest remaining carbon sinks, despite the disturbance episode.

At the regional scale, NEP is estimated to be 5.9 Tg C yr<sup>-1</sup>, or about 28.5 g C m<sup>-2</sup> yr<sup>-1</sup> averaged for the 2.1 × 10<sup>7</sup> ha forest (Table 3). Recently undisturbed forests are the region’s main terrestrial carbon sink, with a NEP of 13.6 ± 3.7 Tg C yr<sup>-1</sup>. In contrast, NEP for forests disturbed by harvest, fire, and bark beetles within the prior two and a half decades are estimated to be -6.4 ± 2.3, -0.5 ± 0.2, and -0.8 ± 0.0 Tg C yr<sup>-1</sup>, respectively, serving as significant carbon sources. Table 3 also reports mean NEP by forest-type group for all forestland and separately for undisturbed and disturbed forests. Fir–spruce–mountain hemlock followed by Douglas-fir and hemlock–Sitka spruce were the largest carbon sinks with 1.6, 1.5, and 1.5 Tg C yr<sup>-1</sup>, respectively. Considering only undisturbed forestlands, Douglas-fir was the largest carbon sink with 7.9 ± 2.1 Tg C yr<sup>-1</sup>, but this was mostly offset by it also having the region’s largest carbon sources from harvest, fire events, and bark beetle outbreaks, with NEP of -5.7 ± 1.6, -0.4 ± 0.1, and -0.2 ± 0.0 Tg C yr<sup>-1</sup>, respectively. Douglas-fir’s relatively large area-integrated carbon fluxes result not only from it being the most abundant forest type in the PNW region, but also because of its large

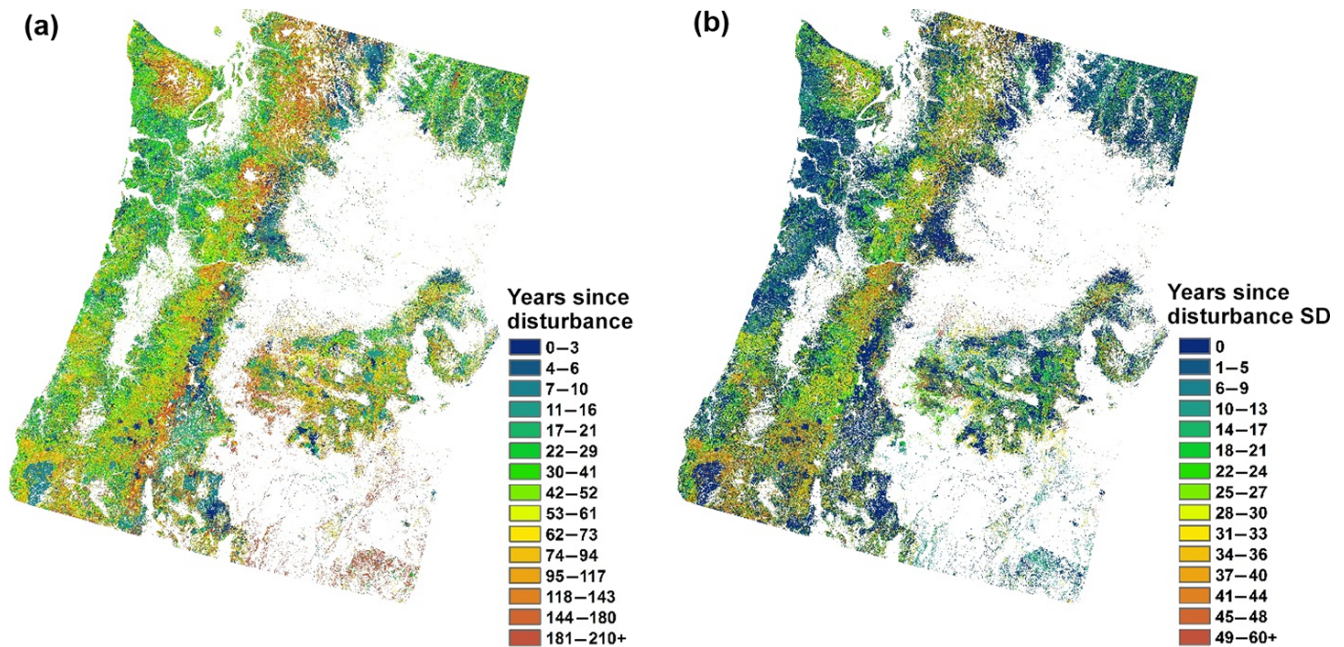


**Figure 7.** Maps of (a) years since disturbance and (b) standard deviation in 2010 in the PNW region.

disturbed areas and large carbon stock potential. Recently disturbed forests tend to aggregate to carbon sources. In some forest-type groups we found a net carbon sink even for recently disturbed forests. For example, lodgepole pine had net carbon sinks for harvested and burned stands. This resulted from a large proportion of disturbance events having occurred early in the disturbance record, allowing recovery and regrowth to overwhelm the carbon sources from the most recent events.

## 4 Discussion

### 4.1 Assumptions of method for mapping time since disturbance and NEP

Our method of inferring time since disturbance to estimate carbon flux and biomass accumulation relies on a number of data products and assumptions that need to be critically evaluated. First, the method assumes that field inventory data provide a reliable and well-constrained estimation of forest biomass as a function of stand age for regionally specific strata of forest type and site-productivity class. However, both stand age and biomass are difficult to measure and estimate, especially considering the difficulty of assigning a stand age to unevenly aged forest stands, as well as selecting appropriate species-specific biomass equations (Parresol, 1999). If FIA ages are older than actual stand ages, the associated forest biomass will be underestimated, and stand age inferred from biomass products will be overestimated. Likewise, FIA ages younger than actual ages will result in an

overestimation in biomass accumulation, but an underestimation in biomass-inferred stand ages. Though a bias in stand ages is possible, our estimates of carbon stocks and fluxes are not likely to be largely adjusted by a stand-age bias within 5 years (Williams et al., 2012).

Second, we assume RS-derived NBCD biomass products were well calibrated by field-derived biomass. However, the correlation coefficients between observed and predicted biomass were estimated to be 0.62–0.75 in the PNW region (Kelldorfer et al., 2013). At the 30 m pixel level, NBCD biomass values were biased, with a large number of zero biomass values that had predictions in local biomass products (Huang et al., 2015). Discrepancies in biomass values between RS- and field-derived data lead to biased estimates in stand age and associated carbon stocks and fluxes. These were addressed in this study by imposing 20 % error on pixel-level biomass estimates and replacing zero biomass with the mean biomass of neighboring forest pixels of the same forest type and site productivity.

Third, the approach described here assumes that stand-level biomass is a useful predictor of stand age, biomass accumulation, and net carbon flux regardless of how that stand-level biomass was actually achieved (Zhang et al., 2014). However, a particular stand-level biomass may be reached from steady accumulation during a relatively disturbance-free interval of time, or from a decline in biomass accumulation after the biomass reaches the maximum, or from a previous disturbance that reduced biomass and then accumulated to the current level (Xu et al., 2012). Information is also lacking on how the biomass–age relationship varies depending on the type of stand-replacing disturbance. Such path depen-

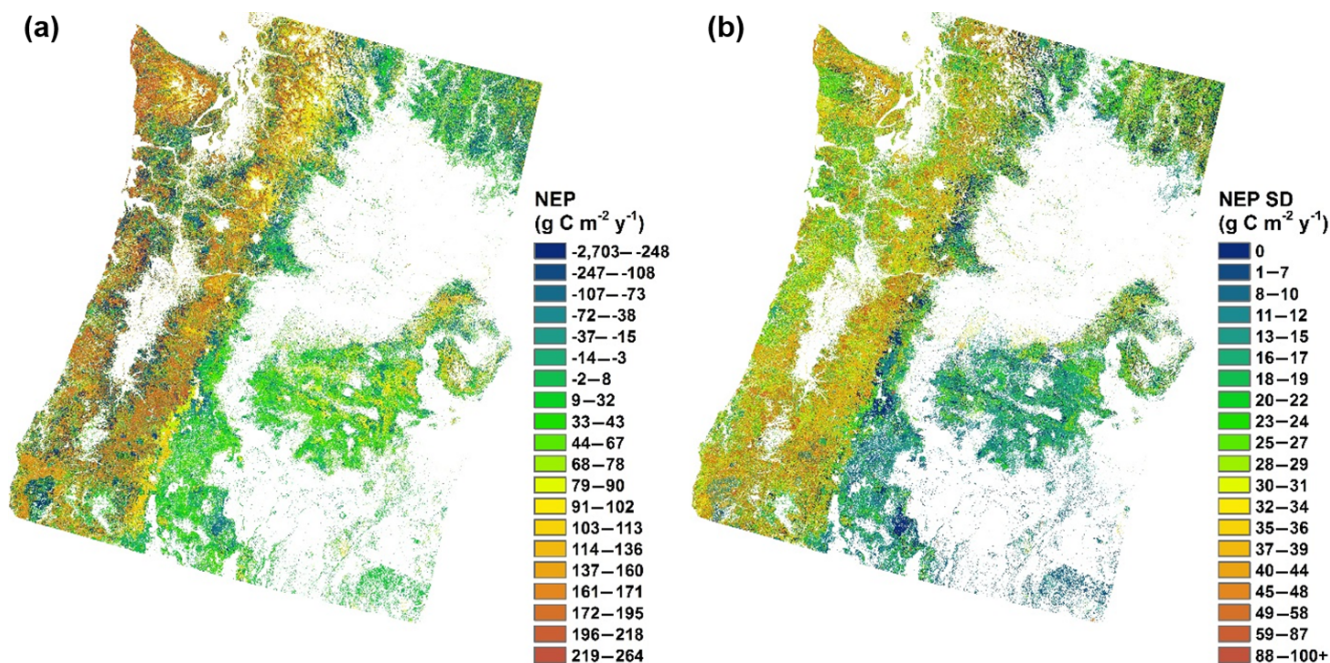


Figure 8. Maps of (a) net ecosystem productivity (NEP) and (b) standard deviation in 2010 in the PNW region.

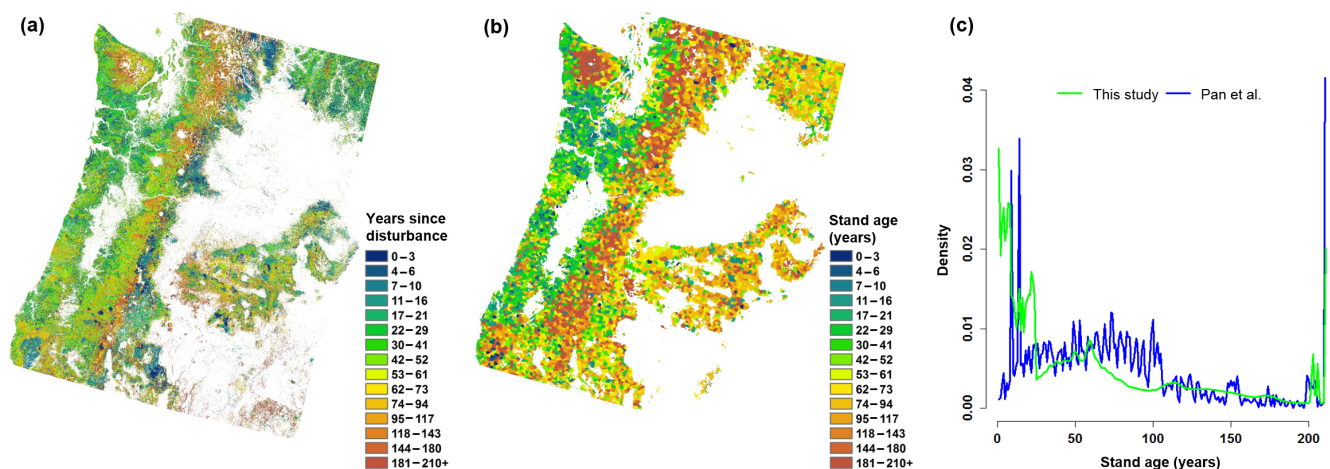


Figure 9. Maps of time since disturbance from (a) this study (same as Fig. 7a) and stand age from (b) Pan et al. (2011) in the PNW region. Associated density curves of stand age are plotted in (c).

density can have important implications for the true stand age as well as for post-disturbance carbon fluxes and stocks by influencing species composition, stand structure, site fertility, and other relevant factors (Williams et al., 2012).

Next, the carbon cycle model used to estimate carbon fluxes as a function of time since disturbance relies on a simple growth rate equation to characterize biomass accumulation over time with a constant wood turnover time, regardless of stand age, and a constant rate of carbon allocation to wood. It also assumes that mean annual net primary productivity is constant after an initial rise through stand initiation (8 years

of initialization is assumed in the model). These assumptions arise from limited data for describing these dynamics for the range of settings active at a continental scale but improvement may be possible with detailed explorations into regional parameterizations. Our prior work indicated some sensitivity of carbon flux estimation to these assumptions, though the impact on continental-scale carbon flux estimation was modest (Williams et al., 2012).

Finally, the method relies on maps of above-ground biomass, forest-type group, site-productivity class, and forest disturbance, which are sure to have errors. Accuracies

of biomass and forest-type group maps were assessed and provided by the data provider, while the rest of them were not. Accuracy of forest-type group maps in the PNW region ranges from 61 to 69 % (Ruefenacht et al., 2008); furthermore, forest-type groups for some pixels undefined from original data were assigned as the forest types of the nearest pixels. For the same biomass value, inferred stand age and estimated carbon fluxes can vary greatly given differences in forest-type group (Figs. 4 and 6); however, NEP biases induced by forest-type group were not accounted for due to lack of information on associated errors from the spatial assignment of forest-type group. The ADS dataset is known to be limited by the areas flown in the survey years, and it likely underestimates the number of trees killed by bark beetles but overestimates the area of affected stands (Meddens et al., 2012). Uncertainties in the ADS dataset have important consequences for the carbon balance and flux estimates from bark beetle outbreaks, part of which was accounted for by Ghimire et al. (2015). Incorporation of local high-resolution high-accuracy maps for these strata into national maps can significantly reduce uncertainties in our mapping and interpretation of stand age, carbon accumulation, and fluxes at fine scales (Huang et al., 2015).

Our analyses have sought to incorporate three main sources of uncertainties in input data layers to estimate mean annual NEP for a given pixel. The first is uncertainty in the biomass defined at the pixel scale. The second source of uncertainty comes from a range of potential stand ages that could correspond to a given biomass stock. The third source of uncertainty comes from the NEP that we estimate for a given stand age, forest type, site productivity, and prior disturbance type and severity. The first and second uncertainties were propagated to provide a probabilistic, statistical estimation of stand age. The full-range distribution of stand age and the third uncertainty were further propagated by probabilistic sampling to obtain an NEP distribution for each forest pixel. The potential biases in NEP due to those uncertainties were reflected by the standard deviation map of NEP in Fig. 8b. Though pixel-level accuracies are correspondingly low for many situations, aggregation to larger scales involves spatial cancellation such that regional and continental uncertainties are much reduced relative to what would be inferred directly from the pixel scale.

#### 4.2 Comparing maps of time since disturbance to other studies

We identified disagreements in density curves derived from the time since disturbance map in this study and the stand-age map in Pan et al. (2011) for the age classes of 0–10 and 50–100 years (Fig. 9c). There are a number of likely explanations for these discrepancies. The first is definitional; in this study we estimated time since disturbance including both partial and stand-replacing disturbances, resulting in assigning a young age to an old-growth forest stand undergoing

a light-severity partial disturbance, while Pan et al. (2011) mapped stand age with consideration of only stand-clearing disturbances. The second cause could be related to the years included in each study, with a large percent of forestlands disturbed by harvest, fire, or bark beetles between 2000 (mapping year in Pan's study) and 2010 (mapping year in this study; Fig. 5). Other factors that may contribute to this discrepancy include different datasets and methodologies used for analysis and mapping, and different spatial resolutions between the maps. For example, when mapping at a much coarser resolution (250 m or 1 km), fragmented disturbed forest patches are likely lost due to disturbed areas taking up a small fraction in the coarse-scale pixel, yielding a stand age for those areas that is represented by nearby undisturbed forest stands that are more abundant in that pixel. The definition bias described above also helps explain partially inconsistent distribution of forest area with age class in this study from the FIA dataset (Fig. 10). In this study, we included partial low-severity disturbances from stands with ages ranging from 0 to 24 years, but which are described as undisturbed forests of older stand age from 20 to 40 years up to 200+ years in the FIA dataset. FIA data miss some recent disturbances, partly because FIA remeasurement cycle in the PNW region is about 10 years, with the average time lag of the data being around 5 years. We note that this definitional issue does bias estimates of NEP or biomass, which are derived based on severity-specific carbon stock and flux trajectories.

The map of time since disturbance from this study, with a spatial resolution of 30 m, is able to distinguish finer differences in the stand-age structure for persistent forests, but it is also able to capture abrupt discontinuities related to recent stand-replacement disturbances, transitions between forest types, and transitions between site-productivity class abundances. This fine spatial detail of the data indicates the information that is lost when stand age is spatially averaged to coarser grids. Such spatial averaging of stand age becomes even more problematic when combined with the nonlinear relationships between forest properties and age, such as with biomass and NEP. Maps of time since disturbance and uncertainties from this study may be valuable for various ecological applications even if our purpose was to generate them as an intermediate variable needed for accurate description and interpretation of carbon stocks and fluxes.

#### 4.3 Comparing maps of NEP to other studies

The PNW-wide forest NEP reported here ( $6 \text{ Tg C yr}^{-1}$ ) is lower than in our earlier work ( $11 \text{ Tg C yr}^{-1}$ ) that used similar methods (see RS-based results in Williams et al., 2014). A portion of this difference can be attributed to larger net carbon losses from forestlands ( $-7 \text{ Tg yr}^{-1}$  carbon loss in this study vs.  $-4 \text{ Tg yr}^{-1}$  carbon loss in Williams et al.) due to recent (1986 to 2010) disturbance by either harvest or fire. Here we also include additional net carbon losses from bark beetle outbreaks ( $-0.8 \text{ Tg C yr}^{-1}$ ) that were not considered in our

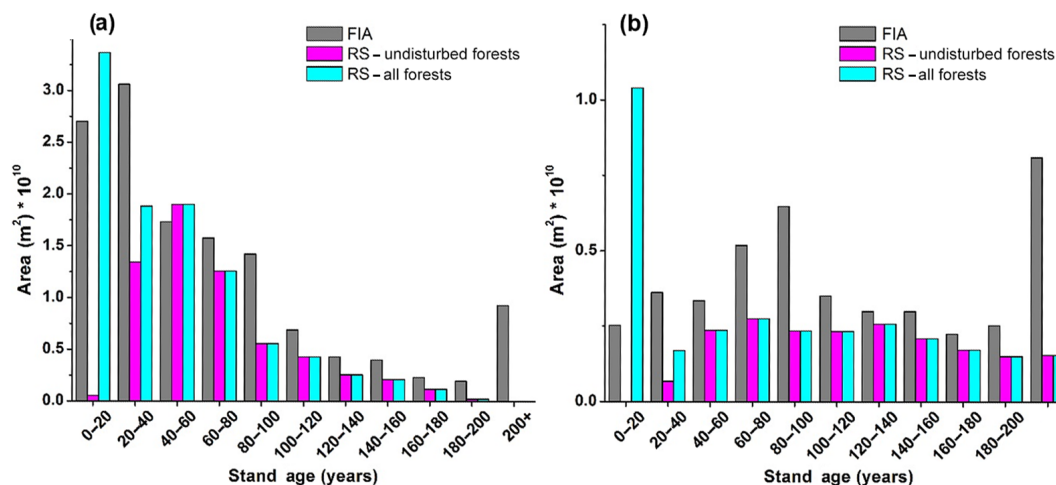


**Figure 10.** Distribution of forest area by age for (a) Douglas-fir and (b) fir–spruce–mountain hemlock of the PNW region comparing results from FIA data and remote-sensing-derived (RS) estimates for undisturbed and all forests, including those marked as disturbed in NAFD, ADS, and MTBS datasets and shown here as if they were stand-clearing events.

earlier work. The remaining discrepancy ( $-1.2 \text{ Tg C yr}^{-1}$ ) may be due to other methodological and data source innovations introduced here, including (1) use of the newly available Landsat-derived forest-disturbance product that now offers full spatial coverage, compared to only about 50 % coverage previously, and (2) new use of biomass data to characterize stand age and associated carbon flux patterns.

The net carbon release from recent bark beetle outbreaks ( $-0.8 \text{ Tg C yr}^{-1}$  in 2010) is comparable to that reported in our earlier work (Ghimire et al., 2015). In our earlier work we reported that the PNW region contributed about 28 % to the net carbon release in western US regions. Applying that percentage to the US western-wide NEP reduction of 1.8 to  $3.6 \text{ Tg C yr}^{-1}$  (Ghimire et al., 2015) indicates a NEP reduction for just the PNW of about  $0.5$  to  $1.0 \text{ Tg C yr}^{-1}$ , within the range of the net carbon release induced by bark beetles reported here.

Additional points of comparison come from a variety of papers focused on regions of Oregon by Turner et al. (2004, 2007, 2015). These studies report similar west vs. east patterns of NEP across the mountain ranges of the region and similar variation in NEP across forest types. However, the work of Turner et al. (2004, 2007 & 2015) tends to estimate higher NEP in regenerating forests (e.g., 14 to 99 years since stand clearing) reaching 250 to  $390 \text{ g C m}^{-2} \text{ yr}^{-1}$  in the Coast Range and Western Cascades, whereas our curves peak at around  $245 \text{ g C m}^{-2} \text{ yr}^{-1}$  for the full PNW region (Fig. S2). This discrepancy could be due to the greater spatial detail of climate patterns included in their modeling work and also because of plant productivity, allocation, and turnover rates prescribed at the ecoregion scale in the work of Turner et al. (2004, 2007, 2015). Given our work's aim of estimating forest carbon stocks and fluxes across the full conterminous US, it is not currently feasible to assemble the

data needed to perform such fine-scale ecoregional calibration even while appreciating its value.

## 5 Conclusions

In this paper, we introduced a new methodology for comprehensively combining RS-based 30 m resolution data on disturbance year, disturbance type, and above-ground biomass with forest inventory data to quantify time since disturbance and associated carbon uptake and release across forested landscapes at a fine scale (30 m). Time since disturbance was an important intermediate variable that aided the assessment of disturbance-driven carbon emissions and removal legacies. We mapped mean, standard deviation, and statistical distribution of stand age and NEP that were propagated from uncertainties in input data layers by probabilistic sampling. This method was applied to the Pacific Northwest (PNW) region of the US. Region-wide we found a net ecosystem productivity of  $5.9 \text{ Tg C yr}^{-1}$  for forestlands circa 2010, with net uptake in undisturbed forests during 1986–2010 ( $13.6 \text{ Tg C yr}^{-1}$ ) overwhelming net negative NEP from tracts that saw recent harvest ( $-6.4 \text{ Tg C yr}^{-1}$ ), fires ( $-0.5 \text{ Tg C yr}^{-1}$ ), and bark beetle outbreaks ( $-0.8 \text{ Tg C yr}^{-1}$ ). Our proposed approach will be further applied to forestlands in other regions of the conterminous US to advance a more comprehensive monitoring, mapping, and reporting of the carbon consequences of forest change across the US.

## 6 Data availability

Data are available upon request.

The Supplement related to this article is available online at doi:10.5194/bg-13-6321-2016-supplement.

*Acknowledgements.* This study was financially supported by NASA's Carbon Monitoring System program (NNH14ZDA001N-CMS) under award NNX14AR39G. Thanks to Yu Zhou for the helpful discussions on carbon flows in the CASA model. Thank you to the associate editor and the two anonymous reviewers for their helpful comments to greatly improve our paper.

Edited by: M. Williams

Reviewed by: two anonymous referees

## References

- Bradford, J. B., Birdsey, R. A., Joyce L. A., and Ryan M. G.: Tree age, disturbance history, and carbon stocks and fluxes in sub-alpine Rocky Mountain forests, *Glob. Change Biol.*, 14, 2882–2897, 2008.
- Chapin III, F. S., Matson, P. A., and Mooney, H. A.: *Principles of Terrestrial Ecosystem Ecology*, 2nd Edn. Springer, New York, 2012.
- Chen, J. M., Ju, W., Cihlar, J., Price, D., Liu, J., Chen, W., Pan, J., Black, A., and Barr, A.: Spatial distribution of carbon sources and sinks in Canada's forests based on remote sensing, *Tellus*, 55, 622–641, 2003.
- Chen, W., Chen, J. M., Price, D. T., and Cihlar, J.: Effects of stand age on net primary productivity of boreal black spruce forests in Canada, *Can. J. Forest Res.*, 32, 833–842, 2002.
- Cohen, W. B., Spies, T. A., and Fiorella, M.: Estimating the age and structure of forests in a multi-ownership landscape of western Oregon, USA, *Int. J. Remote Sens.*, 16, 721–746, 1995.
- Cohen, W. B., Harmon, M. E., Wallin, D. O., and Fiorella, M.: Two decades of carbon flux from forests of the Pacific Northwest, *BioScience*, 46, 836–844, 1996.
- Cohen, W. B., Spies, T. A., Alig, R. J., Oetter, D. R., Maiersperger, T. K., and Fiorella, M.: Characterizing 23 years (1972–95) of stand replacement disturbance in western Oregon forests with Landsat imagery, *Ecosystems*, 5, 122–137, doi:10.1007/s10021-001-0060-X, 2002.
- Eidenshink, J., Schwind, B., Brewer, K., Zhu, Z., Quayle, B., and Howard, S.: A project for monitoring trends in burn severity, *Fire Ecol.*, 3, 3–21, 2007.
- Forest Inventory & Analysis (FIA): USDA Forest Service National Core Field Guide Version 7.0., available at: <http://www.fia.fs.fed.us/library/field-guides-methods-proc/docs/2015/Core-FIA-FG-7.pdf>, last access: 1 August 2015.
- Ghimire, B., Williams, C. A., Collatz, G. J., and Vanderhoof, M.: Fire-induced carbon emissions and regrowth uptake in western US forests: documenting variation across forest types, fire severity, and climate regions, *J. Geophys. Res.-Biogeo.*, 117, G03036, doi:10.1029/2011JG001935, 2012.
- Ghimire, B., Williams, C. A., Collatz, G. J., Vanderhoof, M., Rogan, J., Kulakowski, D., and Masek, J. G.: Large carbon release legacy from bark beetle outbreaks across Western United States, *Glob. Change Biol.*, 21, 3087–3101, doi:10.1111/gcb.12933, 2015.
- Goward, S. N., Masek, J. G., Cohen, W. B., Moisen, G., Collatz, G. J., Healey, S., Houghton, R. A., Huang, C., Kennedy, R. E., Law, B. E., Powell, S., Turner, D. P., and Wulder, M. A.: Forest disturbance and North American carbon flux, *EOS Transactions, Am. Geophys. Union*, 89, 105–106, 2008.
- Goward, S. N., Huang, C., Zhao, F., Schleeweis, K., Rishmawi, K., Lindsey, M., Dungan, J. L., and Michaelis, A.: NACP NAFD Project: Forest Disturbance History from Landsat, 1986–2010, ORNL DAAC, Oak Ridge, Tennessee, USA, doi:10.3334/ORNLDAAC/1290, 2015.
- Huang, C., Goward, S. N., Masek, J. G., Gao, F., Vermote, E. F., Thomas, N., Schleeweis, K., Kennedy, R. E., Zhu, Z., Eidenshink, J. C., and Townshend, J. R. G.: Development of time series stacks of Landsat images for reconstructing forest disturbance history, *Int. J. Digital Earth*, 2, 195–218, 2009.
- Huang, C., Goward, S. N., Masek, J. G., Thomas, N., Zhu, Z., and Vogelmann, J. E.: An automated approach for reconstructing recent forest disturbance history using dense Landsat time series stacks, *Remote Sens. Environ.*, 114, 183–198, 2010.
- Huang, W., Swatantran, A., Johnson, K., Duncanson, L., Tang, H., O'Neil-Dunne, J., Hurtt, G., and Dubayah, R.: Local discrepancies in continental scale biomass maps: a case study over forested and non-forested landscapes in Maryland, USA, *Carbon Balance Manage.*, 10, 19, doi:10.1186/s13021-015-0030-9, 2015.
- Jenny, H.: *The Soil Resources: Origin and Behavior*, Springer-Verlag, New York, 1980.
- Johnson, C. M., Zarin, D. J., and Johnson, A. H.: Post-disturbance aboveground biomass accumulation in global secondary forests, *Ecology*, 81, 1395–1401, 2000.
- Kellndorfer, J., Walker, W., Kirsch, K., Fiske, G., Bishop, J., LaPoint, L., Hoppus, M., and Westfall, J.: NACP Aboveground Biomass and Carbon Baseline Data, V. 2 (NBCD 2000), USA, 2000, from ORNL DAAC, Oak Ridge, Tennessee, USA doi:10.3334/ORNLDAAC/1161, 2013.
- Law, B. E., Turner, D., Campbell, J. L., Sun, O. J., Van Tuyl, S., Ritts, W. D., and Cohen, W. B.: Disturbance and climate effects on carbon stocks and fluxes across Western Oregon USA, *Glob. Change Biol.*, 10, 1429–1444, doi:10.1111/j.1365-2486.2004.00822.x, 2004.
- Liu, S., Bond-Lamberty, B., Hicke, J. A., Vargas, R., Zhao, S., Chen, J., Edburg, S. L., Hu, Y., Liu, J., McGuire, A. D., Xiao, J., Keane, R., Yuan, W., Tang, J., Luo, Y., Potter, C., and Oeding, J.: Simulating the impacts of disturbances on forest carbon cycling in North America: Processes, data, models, and challenges, *J. Geophys. Res.-Biogeo.*, 116, G00K08, doi:10.1029/2010JG001585, 2011.
- Masek, J. G. and Collatz, G. J.: Estimating forest carbon fluxes in a disturbed southeastern landscape: Integration of remote sensing, forest inventory, and biogeochemical modelling, *J. Geophys. Res.-Biogeo.*, 111, G01006, doi:10.1029/2005JG000062, 2006.
- Meddens, A. J. H., Hicke, J. A., and Ferguson, C. A.: Spatial and temporal patterns of observed bark beetle-caused tree mortality in British Columbia and western US, *Ecol. Appl.*, 22, 1876–1891, 2012.
- Pan, Y., Chen, J. M., Birdsey, R., McCullough, K., He, L., and Deng, F.: Age structure and disturbance legacy of North American forests, *Biogeosciences*, 8, 715–732, doi:10.5194/bg-8-715-2011, 2011.

- Parresol, B. R.: Assessing tree and stand biomass: A review with examples and critical comparisons, *Forest Sci.*, 45, 573–593, 1999.
- Randerson, J. T., Thompson, M. V., and Malmstrom, C. M.: Substrate limitations for heterotrophs: Implications for models that estimate the seasonal cycle of atmospheric CO<sub>2</sub>, *Global Biogeochem. Cy.*, 10, 585–602, 1996.
- Raymond, C. L., Healey, S., Peduzzi, A., and Patterson, P.: Representative regional models of post-disturbance forest carbon accumulation: Integrating inventory data and a growth and yield model, *Forest Ecol. Manage.*, 336, 21–34, 2015.
- Ruefenacht, B., Finco, M. V., Nelson, M. D., Czaplowski, R., Helmer, E. H., Blackard, J. A., Holden, G. R., Lister, A. J., Salajanu, D., Weyermann, D., and Winterberger, K.: Conterminous U.S. and Alaska Forest Type Mapping Using Forest Inventory and Analysis Data, *Photogramm. Eng. Rem. S.*, 74, 1379–1388, 2008.
- Saatchi, S., Harris, N. L., Brown, S., Lefsky, M., Mitchard, E. T. A., Salas, W., Zutta, B. R., Buermann, W., Lewis, S. L., Hagen, S., Petrova, S., White, L., Silman, M., and Morel, A.: Benchmark map of forest carbon stocks in tropical regions across three continents, *P. Natl. Acad. Sci. USA*, 108, 9899–9904, 2011.
- Schoennagel, T., Veblen, T. T., and Romme, W. H.: The interaction of fire, fuels, and climate across Rocky Mountain forests, *BioScience*, 54, 661–676, 2004.
- Turner, D. P., Guzy, M., Lefsky, M. A., Ritts, W. D., Van Tuyl, S., and Law, B. E.: Monitoring forest carbon sequestration with remote sensing and carbon cycle modeling, *Environ. Manage.*, 4, 457–466, 2004.
- Turner, D. P., Ritts, W. D., Law, B. E., Cohen, W. B., Yang, Z., Hudiburg, T., Campbell, J. L., and Duane, M.: Scaling net ecosystem production and net biome production over a heterogeneous region in the western United States, *Biogeosciences*, 4, 597–612, doi:10.5194/bg-4-597-2007, 2007.
- Turner, D. P., Ritts, W. D., Kennedy, R. E., Gray, A. N., and Yang, Z.: Effects of harvest, fire, and pest/pathogen disturbances on the West Cascades ecoregion carbon balance, *Carbon Balance and Management*, 10, 12, doi:10.1186/s13021-015-0022-9, 2015.
- Turner, M. G.: Disturbance and landscape dynamics in a changing world, *Ecology*, 91, 2833–2849, 2010.
- Vanderhoof, M., Williams, C. A., Shuai, Y., Jarvis, D., Kulakowski, D., and Masek, J.: Albedo-induced radiative forcing from mountain pine beetle outbreaks in forests, south-central Rocky Mountains: magnitude, persistence, and relation to outbreak severity, *Biogeosciences*, 11, 563–575, doi:10.5194/bg-11-563-2014, 2014.
- Williams, C. A., Collatz, G. J., Masek, J., and Goward, S. N.: Carbon consequences of forest disturbance and recovery across the conterminous United States, *Global Biogeochem. Cy.*, 26, GB1005, doi:10.1029/2010GB003947, 2012.
- Williams, C. A., Collatz, G. J., Masek, J., Huang, C., and Goward, S. N.: Impacts of disturbance history on forest carbon stocks and fluxes: merging satellite disturbance mapping with forest inventory data in a carbon cycle model framework, *Remote Sens. Environ.*, 151, 57–71, 2014.
- Williams, C. A., Gu, H., MacLean, Masek, J., and Collatz, G. J.: Disturbance and the carbon balance of US forests: A quantitative review of impacts from harvests, fires, insects, and droughts, *Global Planet. Change*, 143, 66–80, 2016.
- Wilson, B. T., Woodall, C. W., and Griffith, D. M.: Imputing forest carbon stock estimates from inventory plots to a nationally continuous coverage, *Carbon Balance Manage.*, 8, 1, doi:10.1186/1750-0680-8-1, 2013.
- Xu, C., Turnbull, M. H., Tissue, D. T., Lewis, J. D., Carson, R., Schuster, W. S. F., Whitehead, D., Walcroft, A. S., Li, J., and Griffin, K. L.: Age-related decline of stand biomass accumulation is primarily due to mortality and not to reduction in NPP associated with individual tree physiology, tree growth or stand structure in a *Quercus*-dominated forest, *J. Ecol.*, 100, 428–440, doi:10.1111/j.1365-2745.2011.01933.x, 2012.
- Zhang, F., Chen, J. M., Pan, Y., Birdsey, R. A., Shen, S., Ju, W., and He, L.: Attributing carbon changes in conterminous US forests to disturbance and non-disturbance factors from 1901 to 2010, *J. Geophys. Res.-Biogeo.*, 117, G02021, doi:10.1029/2011JG001930, 2012.
- Zhang, C., Ju, W., Chen, J. M., Li, D., Wang, X., Fan, W., Li, M., and Zan, M.: Mapping forest stand age in China using remotely sensed forest height and observation data, *J. Geophys. Res.-Biogeo.*, 119, 1163–1179, doi:10.1002/2013JG002515, 2014.
- Zhu, Z., Woodcock, C. E., and Olofsson, P.: Continuous monitoring of forest disturbance using all available Landsat imagery, *Remote Sens. Environ.*, 122, 75–91, 2012.